University of Baghdad
College of Engineering
JE
JOURNAL OF ENGINEERING

Journal of Engineering

journal homepage: www.jcoeng.edu.iq

Volume 30 Number 7 July 2024

Design and Implementation of a Microstrip Six-Port Reflectometer (SPR) with Enhanced Bandwidth

Nadine Adnan Shaaban [1,*], Ghassan Nihad Jawad[2]

Department of Electronic and Communications Engineering, College of Engineering, University of Baghdad, Baghdad, Iraq
nadeen.adnan2106m@coeng.uobaghdad.edu.iq[1], ghassan.jawad@coeng.uobaghdad.edu.iq[2]

ABSTRACT

A compact microstrip six-port reflectometer (SPR) with extended bandwidth is proposed in this paper. The design is based on using 16-dB multi-section coupled line directional couplers and a multi-section 3-dB Wilkinson power divider operating from 1 to 6 GHz. The proposed SPR employs only two calibration standards: a matched load and an open load. As compared to other dielectric substrates, fabricating the proposed SPR involves using a low-cost (FR4) substrate. A novel algorithm is also proposed to estimate the complex reflection coefficient over the frequency ranges at which the standard performance of the circuit components is not fully satisfied. The new algorithm is based on the circles' intersection points, which have been derived from basic SPR equations, to estimate the complex reflection coefficient. To validate the SPR performance, a multiband microstrip patch antenna has been measured and the resulted reflection coefficient is compared with those obtained using a vector network analyzer (VNA). Results show that the proposed SPR provides a good estimation of the complex reflection coefficient within the frequency range of 1 GHz to 8 GHz. Owing to its compact size and ease of fabrication, the proposed reflectometer is suitable for various microwave broadband applications.

Keywords: Broadband, Complex reflection coefficient, Coupled-line directional coupler, Six-port reflectometer, Power divider.

*Corresponding author
Peer review under the responsibility of University of Baghdad.
https://doi.org/10.31026/j.eng.2024.07.08

Article received: 12/11/2023
Article accepted: 25/02/2024
Article published: 01/07/2024

تصميم دائرة عاكس موجات دقيقة سداسي البوابات ذو نطاق ترددات عريض

نادين عدنان شعبان*، غسان نهاد جواد

قسم هندسة الالكترونيك والاتصالات، كلية الهندسة، جامعة بغداد، بغداد، العراق

الخلاصة

في هذه الورقة تم اقتراح مقياس انعكاس مدمج لستة منافذ (SPR) مع عرض نطاق ترددي ممتد. يعتمد التصميم على استخدام مقارنات اتجاه الخط متعددة الأقسام ومقسم طاقة ويلكينسون متعدد الأقسام. نوع مقارن الاتجاه الذي تم تصميمه لتوجيه الموجة هو (16-dB). ونوع مقسم طاقة ويلكنسون المستخدم هو (3-dB) والذي يقسم الاشارة القادمة من المدخل بالتساوي وبنفس الزاوية ويعمل ضمن نطاق ترددي من (1-6 GHz). يستخدم SPR معيارين للمعايرة: حمل مطابق وحمل مفتوح. وايضاً تم استخدام عازل نوع (FR4) في عملية التصنيع والذي يمتاز بقلة التكلفة مقارنة بباقي العوازل الاخرى. تم اقتراح خوارزمية جديدة لتقدير معامل الانعكاس المعقد في نطاق الترددات التي لا يتحقق فيها الأداء القياسي لمكونات الدائرة بشكل كامل. تستند الخوارزمية الجديدة لتقدير معامل الانعكاس المعقد بشكل اساسي على نقاط تقاطع الدوائر التي تم اشتقاقها من معادلات SPR. كما تم مقارنة نتائج S-parameters بين المحاكاة وبين المقاسة عملياً. تم التحقق من أداء SPR عن طريق قياس معامل الانعكاس لهوائي متعدد النطاق نوع microstrip ومقارنة النتائج مع تلك التي حصل عليها متجه محلل الشبكة (VNA). تظهر النتائج أن SPR المقترح يوفر تقديرًا دقيقًا لمعامل الانعكاس المعقد ضمن نطاق التردد من 1 جيجاهرتز إلى 8 جيجاهرتز. ونظرا لحجمه المدمج وسهولة تصنيعه، فإن مقياس الانعكاس المقترح مناسب لمختلف تطبيقات النطاق العريض بالموجات الدقيقة.

الكلمات المفتاحية: موجات دقيقة، نطاق ترددي عريض, معامل انعكاس معقد, المقرن الاتجاهي للخط المقترن, مقياس انعكاس سداسي منافذ, مقسم الطاقة.

1. INTRODUCTION

The reflectometer is one of the most effective instruments in microwave metrology. Its main function is to measure the complex reflection coefficient (or the input impedance) of an unknown load. The conventional Vector Network Analyzer (VNA) provides this type of measurement for microwave devices such as antennas, cables, filters, amplifiers, etc. However, VNAs are expensive and bulky since they provide extra functions that are not beneficial for numerous applications that only require measuring the complex reflection coefficient, where an affordable and compact reflectometer can be used.

In the 1970s, the original concepts of a multi-port reflectometer were first introduced by **(Engen, 1977a; Engen, 1977b)**. Such circuits provide a simple measurement of both the magnitude and phase of the complex reflection coefficient (Γ) of a Device Under Test (DUT) by using only a few power measurements. The basic design of a reflectometer has used five directional couplers and more than three calibration standards to test a DUT **(Engen, 1977a)**. Afterwards, improvements in the performance and functionality of the multi-port reflectometer have been proposed in different studies, such as the multi-port circuit proposed in **(Yeo and Lee, 1990)**, which used a symmetrical five-port waveguide junction

with a directional coupler. This configuration satisfied the optimum criteria but suffered from poor matching that affected the reflectometer's performance. Another proposed multiport reflectometer employing the WR15 waveguide design **(Haddadi et al., 2018)**, for the use of near-field sensor applications. This design exhibited better resistance to external impacts in trade-off with circuit size. To improve the reflectometer readings, a six-port reflectometer (SPR) with planar designs has been introduced **(Staszek et al., 2013; Staszek et al., 2016; Ghosh and Kumar, 2017; Staszek et al., 2017b; Hassan and Abbas, 2018; Staszek, 2022)**. The SPR features a simple design as well as affordable components with high-accuracy measurements. For example, to measure the complex reflection coefficient, an SPR was proposed to operate between 2 and 3.5 GHz **(Staszek et al., 2013)**. The suggested design used more than three calibration standards to get the unknown parameters. However, the design has limited bandwidth, making it useful for narrowband applications. Similarly, in **(Staszek et al., 2016; Hassan and Abbas, 2018; Staszek, 2022; Peng et al., 2023)**, the designs operation extended into restricted frequency regions. In **(Staszek et al., 2017b)**, another SPR structure has been presented to operate in the frequency range of 2.2–2.6 GHz. This design used tunable parameters to improve the accuracy of the measurements. Despite good agreement between expectations and measurements, this design suits only applications with limited bandwidth. Another proposed SPR with simple structure aimed for narrowband applications **(Ghosh and Kumar, 2017)** was designed and fabricated with a minimum number of calibration standards and fewer components. Similarly to the simplified configuration in **(Odrobina et al., 2017)**, the design suffered from bandwidth limitations.

To meet the bandwidth criteria, numerous researchers have endeavored to improve the previously-reported designs. For instance, a four-port reflectometer (FPR) has been proposed **(Haddadi et al., 2008)** uses only two power detectors to estimate the value of the complex reflection coefficient. Despite achieving a wideband measurement within the frequency range of 1-4 GHz, the design has resulted in an arduous calibration procedure with eight loads to finish the characterization of the system. Another broadband SPR has been introduced **(Lin et al., 2017)**. This design consisted of five couplers built from nine sections of non-uniform and offset parallel-coupled transmission lines and achieved accurate measurements over a relatively wide frequency range (2–20 GHz). Nevertheless, such a design increases the circuit size and requires stacking and aligning three layers of substrate, which causes fabrication challenges. A strip-line structure with multiple probes distributed along two parallel transmission lines achieved ultra-wideband operation, as has been presented in **(Staszek et al., 2017a)**. However, this design has eight ports, which requires more than five standards for calibration and a consequent increase in calculation complexity. Moreover, the probe placement on the transmission line has proved to be critical for ensuring high measurement accuracy and wide bandwidth. Another structure using strip-line technology has been proposed in **(Odrobina et al., 2018)**. This design consisted of five 3-dB, three-section directional couplers. As an alternative to the Wilkinson power divider, a pair of directional couplers were used. However, a design that uses one power divider and three directional couplers might exhibit better balance for the signal **(Bialkowski et al., 2007)**. Moreover, the strip-line fabrication may encounter challenges in terms of cost compared to the microstrip due to the need for extra layers and vias. To ensure accurate measurements, a seven-port reflectometer has been presented **(Dietrich et al., 2018)**. However, such a design led to a strict calibration procedure. In **(Seman et al., 2008)**, a multi-port reflectometer using multilayer microstrip slot technology is presented. The compact design consisted of nine ports, with a pair of ports connected to a matched load. The operating frequency ranges from 3.1 to 10.6 GHz, making it suitable for ultra-wideband

applications. Despite the multi-layer design decreasing the circuit size and enhancing bandwidth, extra screw holes might be needed, which might increase the fabrication difficulty. Furthermore, it may experience challenges in integration with other planar devices.

Compact design and broadband bandwidth are increasingly required in a variety of applications. For example, broadband wireless applications **(Mohammed et al., 2014; Issa et al., 2022)**, broadband radar sensors and materials **(Ali and Al-Hindawi, 2021; Hathal et al., 2021)**, biomedical applications **(Al-Jumaily and Al-Ammri, 2009; Aishah et al., 2015)**, and imaging systems **(Abbass and Abdulateef, 2012)**. Wideband measurement is also significantly needed in microwave non-destructive testing (MNDT) applications, such as measuring the reflection signal back from internal flaws inside the surface and inspecting its dielectric properties **(Zoughi, 2000; Shrifan et al., 2020; Jawad and Akbar, 2021)**.

In this work, a compact microstrip SPR circuit is proposed to estimate the complex reflection coefficient for unknown loads over a wide frequency range using two calibration standards only. The design approach is based on probing the incident and reflected signals along a microstrip line at different locations **(Ghosh and Kumar, 2017)**. However, unlike the previously reported reflectometer **(Ghosh and Kumar, 2017)**, the proposed circuit is modified to increase the bandwidth of the individual components without increasing the overall circuit size. Furthermore, a novel algorithm is proposed to provide an accurate estimation of the complex reflection coefficient within the frequencies where the individual circuit parameters do not comply with the previously set reflectometer design conditions. Applying this algorithm provides a further increase in the operational bandwidth.

2. PROPOSED DESIGN

2.1 The Six-Port Reflectometer Equations

The SPR general block diagram is shown in **Fig. 1**. The passive six-port junction splits an input signal at port 6 (a_6) into five output signals at ports 1, 2, 3, 4, and 5 with different phases and amplitudes. The scalar power of the four output signals (P1-P4) is measured by means of power detectors. One of the detectors is connected to port 2, which serves as a reference port. The DUT, which is the object of interest in the SPR circuit, is connected to port 5.

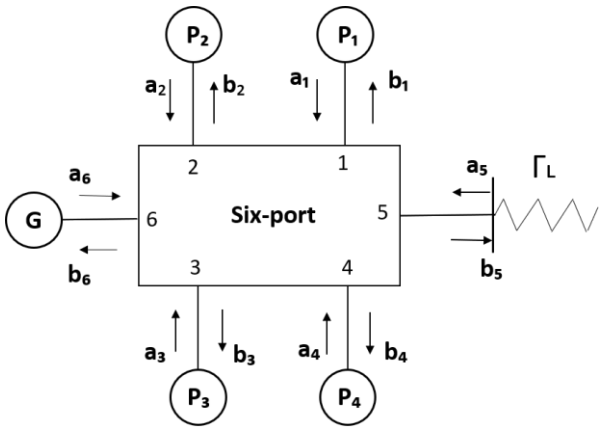

Figure 1. A general block diagram of a six-port reflectometer.

A calibration procedure, where loads with known reflection responses are connected and measured, is usually used to calculate the parameters on which the reflection coefficient estimation process relies.

The SPR circuit can be modelled by a matrix equation that relates the incident and reflected waves at each port. The reflected wave at each port (bi) can be related to the incident wave to the DUT ($b_5 \equiv b$) and the reflected wave from the DUT ($a_5 \equiv a$) by **(Ghannouchi and Mohammadi, 2009)**.

$$b_i = A_i\, a + B_i\, b \qquad i = 1, 2, 3, and\ 4 \tag{1}$$

where A_i and B_i are complex terms that characterize the SPR and represent the entries of the inverse of the matrix equation that depends on its S-parameters. The power detected at each port is proportional to the square of the magnitude of the corresponding wave; therefore:

$$P_i = |b_i|^2 = |A_i\, a + B_i\, b|^2 = |b|^2 |A_i|^2 |\Gamma - Q_i|^2 \tag{2}$$

where $\Gamma = a/b$ is the complex reflection coefficient of the DUT and $Q_i = (-B_i)/A_i$ is a complex constant at port i (where $i = 1, 2, 3, and\ 4$). Normalizing the detected power P_i ($i = 1, 3, and\ 4$) by the reference power at port 2 yields:

$$P_i = \frac{P_i}{P_2} = C_i |\Gamma - Q_i|^2 \qquad i = 1, 3, and\ 4. \tag{3}$$

where $C_i = |A_i/B_2|^2$ are real constants that depend on the SPR circuit parameters. These parameters are referred to as *calibration constants*. They can be obtained by the calibration procedure, in which the DUT is replaced with loads that have a known reflection coefficient (calibration standards) over the desired frequency range. Each equation in Eq. (3) graphically stands for a circle in the complex Γ-plane, where the center is Q_i, the radius is $r_i = \sqrt{P_i/C_i}$, and the solution of Γ is the intersection of the three circles within the region of reflection coefficient unit circle. This means that the solution of Γ should satisfy the condition $|\Gamma| \leq 1$ for a passive DUT. The graphical method provides a useful check on the existence and uniqueness of the solution as well as estimating its value. It can be concluded from the above that it is possible, in concept, to obtain an estimation of the complex reflection coefficient using the intersection of two circles only. The redundant measurement approach of the SPR allows for the estimation of the accuracy of each measurement **(Engen, 1992)**. This is done by a third circle crossing the other two circles at the same point inside the unit circle so that the uncertainty of each measurement can be determined. **Fig. 2(a)** shows the complex Γ-plane, where the ideal placement of the circles has just one intersection that falls within the unit circle. However, in practice, the three circles' intersections form an area that resembles a quasi-triangle, as shown in **Fig. 2(b)**.

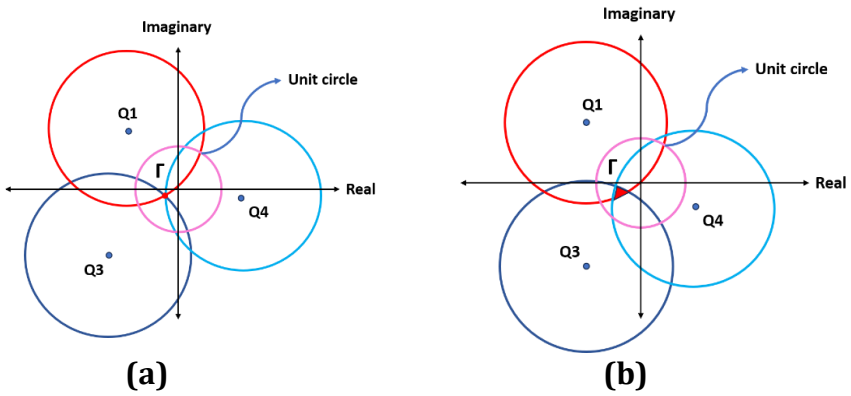

Figure 2. Q-points placement (a) ideal case and (b) practical case

This area should be as small as possible to ensure a more precise estimation. However, real components and detectors have imperfections and nonlinearities that cause the intersection points to deviate from this optimal location **(Brunetti, 1990)**. Consequently, the quasi-triangle area may enlarge and introduce errors as a result of these factors. The operating bandwidth of the SPR is directly related to the position of the circles' centers (Q-points) for all the frequency points of interest. For an accurate estimation, these centers should not be too close to each other **(Brunetti et al., 1989)**, otherwise, the intersections of the circles would be at different locations within (or sometimes outside) the unit circle, and that results in ambiguity and/or instability in the estimation of Γ. Therefore, one of the main challenges in the SPR design is to minimize the variation of the Q-points over a wide frequency range while considering the size of the circuit, the number of components, and the simplicity of the calibration procedure. Another thing to consider is that the radii of the circles depend on the reflected power from the DUT, and errors in estimation might occur if the Q-point locations are too far away from the unit circle.

2.2 The Six-Port Reflectometer Design

A diagram of the proposed microstrip probe-based SPR circuit is shown in **Fig. 3**. It consists of a power divider that splits the input signal at port 6 into two branches: the first feeds port 2 (the reference port), and the other branch ends at the DUT (port 5). Three directional couplers are arranged along the second branch in order to provide access to the power that is related to the incident and reflected waves from the DUT at different locations (ports 1, 3, and 4).

The proposed circuit has been designed after setting specific assumptions and analyzing the design requirements in order to achieve an acceptable estimation of (Γ) within a wide frequency range. This section will highlight these assumptions and requirements and their effect on the design parameters of the main circuit components.

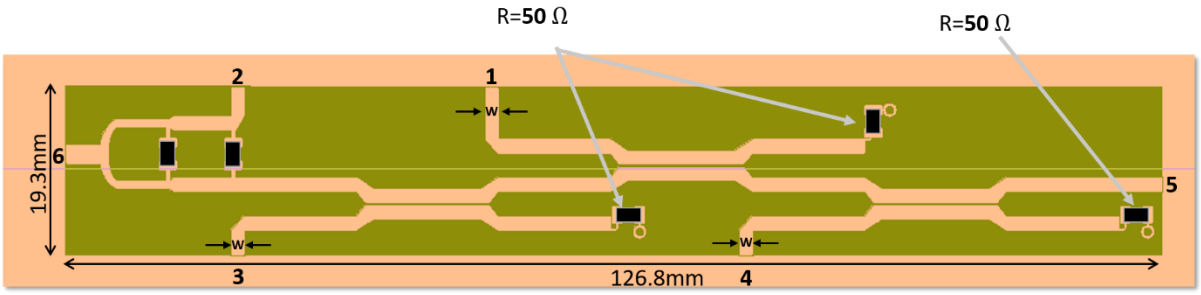

Figure 3. Schematic diagram of the proposed SPR circuit.

2.3 Design Requirements

As illustrated in the previously, the centers of the circles (the Q-points) should be close enough to the unit circle in order to intersect at a single point inside the unit circle and produce a correct estimation of Γ **(Engen, 1977b)**. It has also been reported before **(Ghosh and Kumar, 2017)** that an approximate value of Qi can be determined from $Qi \cong S_{i6}/S_{i5}\,S_{56}$, and acceptable estimations of Γ can be obtained when the magnitude of this value lies between 0.5 and 3. By examining this equation, it can be concluded that the ratio between S_{i6} and S_{i5} has to be approximately maintained within these limits for the widest possible frequency range. In other words, the directional couplers should be carefully designed in order to fulfill this condition. It has also been shown that the angles of the Q points should be equally arranged around the unit circle (ideally, to be 120^0 apart) to guarantee a single intersection inside the unit circle **(Engen, 1977b)**.
Another design requirement is determined by the use of port 2 as a reference port. So the output power should give an indication of only the input power level (from port 6) and shouldn't depend on the reflected power from the DUT (port 5). Consequently, good isolation between the two output ports of the power divider is needed to obtain $A_2 = 0$. Therefore, a simple Y-junction or a resistive power divider cannot be used for this design. Instead, a multi-section Wilkinson power divider should be used to achieve the required isolation between the output ports over a wide frequency range **(Pozar, 2012)**.
Here, the four power meters of the SPR are assumed to be well-matched to their ports. Hence, $\Gamma_i = 0$ for $i = 1,\ 2,\ 3, and\ 4$. This practically achievable assumption simplifies the calibration process and reduces the mismatch errors.

2.4 Calibration Procedure

The complex coefficients Bi and Ai of the SPR circuit are determined from the following equations using two calibration standards: a matched load and an open load **(Ghosh and Kumar, 2017)**:

$$B_{\mathrm{i}} = \frac{S_{\mathrm{i6}}}{S_{56}} \tag{4}$$

$$A_{\mathrm{i}} = \frac{1}{\Gamma_O}\left(\frac{S^O_{\mathrm{i6}}}{b_O} - B_{\mathrm{i}}\right) \tag{5}$$

The parameters S_{i6} and S_{56} are obtained from the load measurement when the matched load is connected to port 5. Next, the open load is connected to port 5, and the incident wave b_O

is derived from this measurement. The reflection coefficient Γ_O is computed from a 50 Ω transmission line that terminates with an open load. Finally, all the obtained parameters of the SPR circuit are processed and used in a new algorithm to find the complex reflection coefficient Γ_L at port 5, as will be shown later.

2.5 Design of a Broadband Wilkinson Power Divider

The power divider used in the proposed design is a 3-dB two-section Wilkinson power divider operating at a frequency range of 1 to 6 GHz **(Mishra et al., 2014)**. The power divider is designed separately using a 0.8 mm-thick FR4 substrate ($\varepsilon_r = 4.4$), as illustrated in **Fig. 4(a)**, which is the same substrate for the whole reflectometer. The power divider consists of two transmission line sections with the specifications listed in **Table 1**. The two isolation resistors are SMD-type, with $R1 = 100\ \Omega$ and $R2 = 200\ \Omega$. The results obtained from simulating the proposed design using CST Microwave Studio software are shown in **Fig. 4(b)**, which indicate good performance in terms of return loss, isolation, and insertion loss up to 6 GHz.

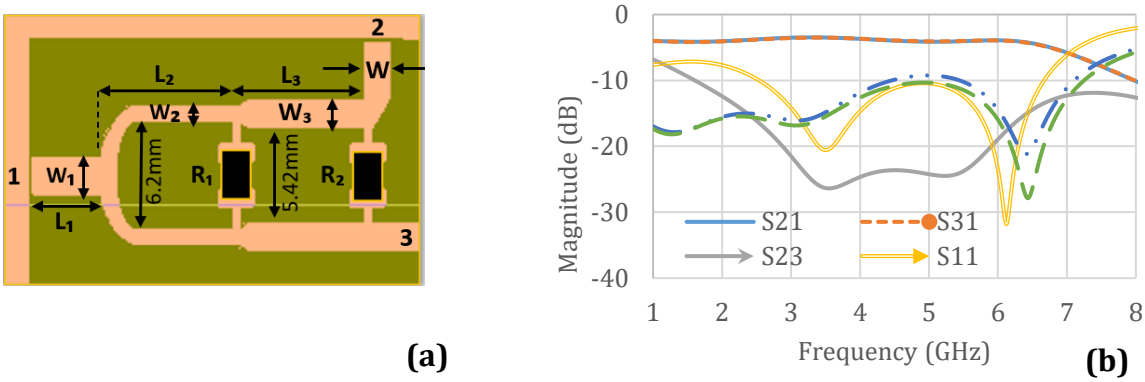

(a) **(b)**

Figure 4. Compact modified multi-section WPD. (a) schematic diagram. (b) simulated scattering parameters.

Despite the increase in reflection and insertion losses above this frequency, the isolation between the two ports is maintained up to 9 GHz, which ensures the isolation of port 2 in the reflectometer. In addition, even when the insertion loss at the input of the circuit is high (for frequencies above 6 GHz), the SPR can still operate since the measured output power at port i $(i = 1, 3, \text{and } 4)$ is normalized with respect to the output power at port 2. The imperfections that result from this extension in frequency are amended by using the proposed algorithm that will be illustrated in the next section. It is worthwhile to note that increasing the number of sections of the power divider can provide a wider bandwidth. However, that will increase the overall size of the reflectometer.

2.6 Design of Directional Couplers

A symmetrical three-section 16-dB coupled-line directional coupler at 3 GHz has been used in the proposed SPR. Even-mode and odd-mode analysis **(Pozar, 2012)** is used in analyzing the coupler design and, hence, to determine the coupling factor of the following sections (C1, C2, and C3). The lengths and widths of each section, in addition to the gaps between the lines, are determined based on the odd- and even-mode analysis illustrated in **(Steer, 2019)**. The directional coupler's schematic diagram is shown in **Fig. 5(a)**, and its design parameters are illustrated in **Table 1**.

Table 1. Design parameters for: multi-section WPD and 16-dB multi-section directional coupler. (All of the dimensions are in millimeters.)

Multi-Section Wilkinson Power Divider				
Length	L1	L2	L3	
	5	7. 0675	7. 0675	
Width	W	W1	W2	W3
	1.52	2.204	0.9	1.682
Resistors	R1		R2	
	100 Ω		200 Ω	
Substrate	Ɛr	Thickness	Loss tangent (tan(δ))	
FR4	4.4	0.8	0.025	
16 dB Multi-Section Directional Coupler				
Length	Lc1	Lc2	Lc3	
	14	14.4	14	
Width	W	Wc1	Wc2	Wc3
	1.52	1.664	1.524	1.664
Space	S1	S2	S3	
	2.77	0.37	2.77	
Substrate	Ɛr	Thickness	Loss tangent (tan(δ))	
FR4	4.4	0.8	0.025	

From the earlier described design considerations, the ratio of the coupling and isolation has to be close to unity in order for the Q points to be near to the unit circle. Here, it can be concluded from **Fig. 5(b)** that the designed directional coupler maintains the ratio between S_{31} and S_{41} approximately close to such values from 1 GHz up to about 5.5 GHz. Beyond this frequency, however, the same ratio fluctuates in value, which would result into unequal values of Q at these frequencies. This limitation has been, so far, the main challenge of maintaining accurate estimation of Γ across a wide frequency range since the standard reflectometer design approach dictates keeping the ratio of coupling to the isolation nearly constant. A novel algorithm is suggested to overcome this limitation and enhance the bandwidth of this design approach, as will be shown in the next section.

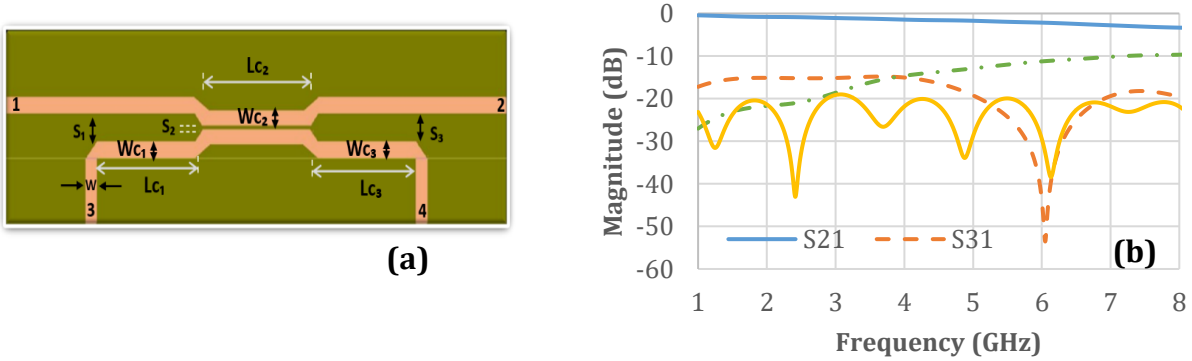

Figure 5. Symmetrical three-section 16 dB coupled-line directional coupler. (a) schematic diagram. (b) simulated scattering parameters.

3. BANDWIDTH ENHANCEMENT ALGORITHM

The proposed algorithm in this work aims to reduce the uncertainty of the complex reflection coefficient measurements over a wide frequency range. The algorithm is applied to find the estimated complex Γ from the intersection of three circles; the center of each circle is determined by their respective Q points, and the radii are obtained from the measured power at the associated port (1, 3, or 4) when the DUT is attached to port 5. As explained before, the ideal situation would yield the three circuits to intersect at a *single point* within the unit circle. However, imperfections in the circles' centers and radii cause the intersections to deviate from each other and reduce the possibility of accurate Γ estimation. The proposed algorithm aims to enhance the estimation method by processing the intersection points in order to find the most accurate estimation of the complex reflection coefficient by applying the following steps (described here for a single frequency point).

- During the calibration process, the Q-points are obtained and split into real and imaginary parts.
- The radii of the circles (r_1, r_3, and r_4) are found from the detected powers and the values of A and B at each port (1, 3, and 4). Thus, three circles in the complex Γ plane can be determined.
- The two circles cross each other at two points in general. After finding these intersections (six in total, regardless of their location with respect to the unit circle), the Euclidean distance between any two intersections is obtained by

$$d = \sqrt{(x_2 - x_1)^2 + (y_2 - y_1)^2} \tag{6}$$

  where (x_1, y_1) and (x_2, y_2) are the coordinates of two intersection points. Twelve distances will yield after excluding the distances between the intersection points that lie on the same circles.
- Next, the calculated distances form eight possible triangles in total. It has been found that the triangle that is more likely to enclose the accurate reflection coefficient point is the one with the smallest perimeter, rather than the smallest area. Therefore, the algorithm finds the three intersection points that form the vortex of the triangle with the smallest perimeter. The centroid of this triangle is calculated by averaging these points, which is the estimated complex reflection coefficient (Γ).

$$\text{Centroid} = \frac{x_1+x_3+x_4}{3}, \frac{y_1+y_3+y_4}{3} \tag{7}$$

where (x_1,y_1), (x_3 , y_3), and (x_4, y_4) are the three vertices of the triangle with the smallest perimeter.

The proposed algorithm has a significant advantage in handling exceptional cases and preserves its integrity over a wide frequency range. For example, the algorithm is able to resolve the case of multiple intersections inside the unit circle (such as the case shown in **Fig. 6(a)**), which has previously limited the estimation process of Γ by treating a single intersection only in this region **(Engen, 1977b)**. Another case is when two Q-points are aligned or centered on the same line, and these two circles do not cross but only touch because they are too sensitive to the changes in the circle radius **(Bilik, 2002)**, as shown in **Fig. 6(b)**.

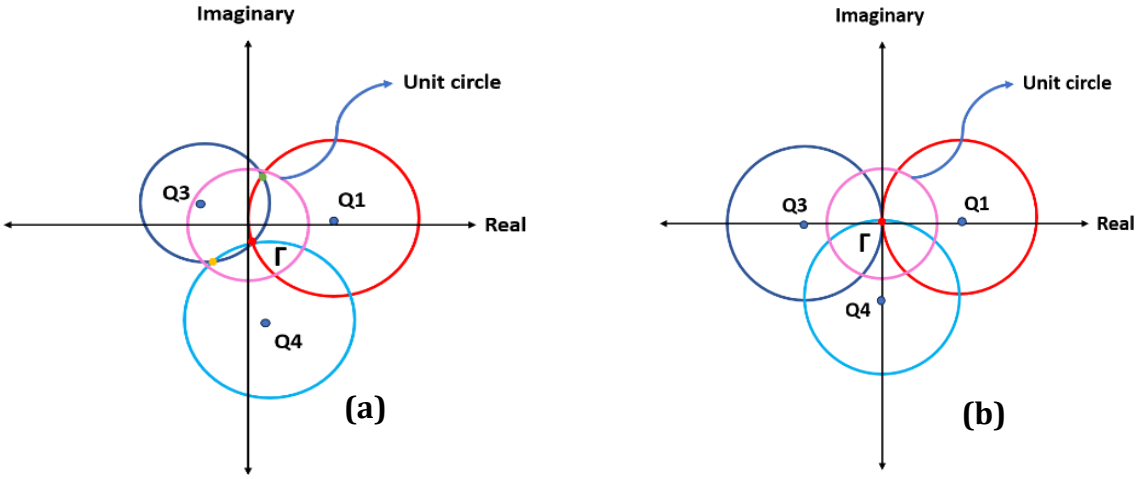

Figure 6. Geometric interpretation of crossing points inside the unit circle: (a) more than one points inside the unit circle. (b) two Q-points are centered on the same line.

The value of Γ will be found by using the average of the two points where the third circle intersects with them but is not centered on the same line. In addition, the algorithm has been adjusted to estimate the value of Γ using only two circles instead of three. This is done when only two circles have a common intersection point, and the third circle does not touch either of them. In this situation, the value of Γ can be obtained from the point where the two circles meet inside the unit circle. Such advantages allow the proposed reflectometer to provide an accurate estimation of Γ within the frequencies where the circuit parameters do not comply with the design requirements illustrated before. The fabricated SPR design is shown in **Fig. 7.**

4. RESULTS AND DISCUSSION

The proposed reflectometer has been simulated, fabricated, and tested using a VNA (Agilent E5071C). **Fig. 8** shows a comparison between the simulated and measured

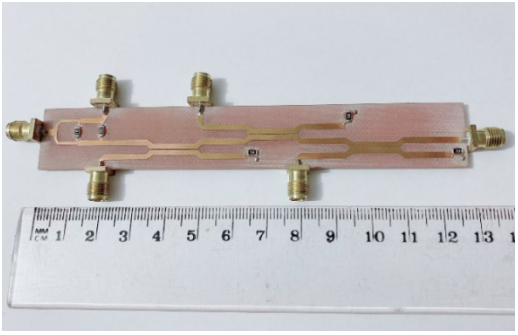

Figure 7. The proposed SPR fabricated design.

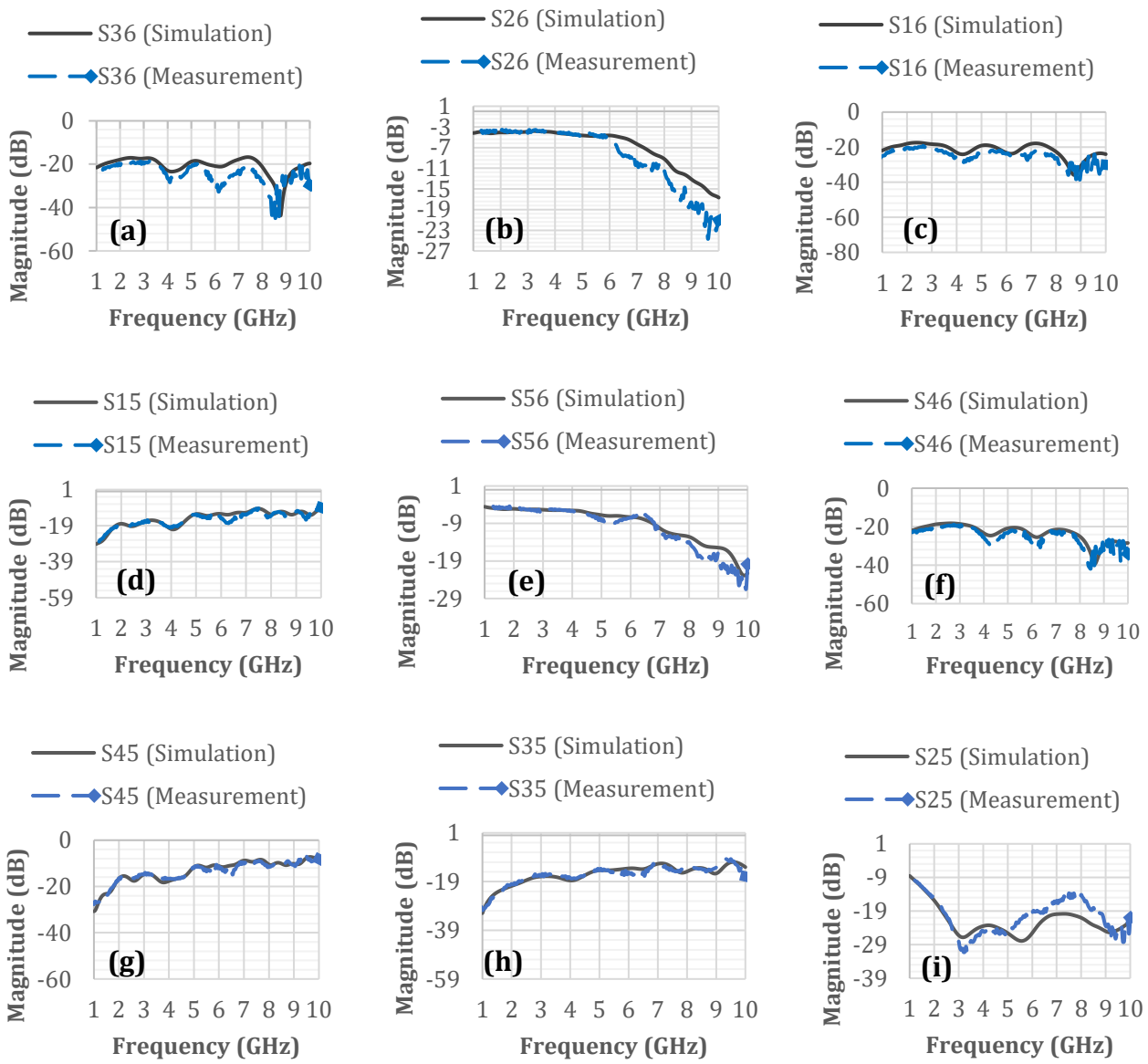

Figure 8. The comparison of simulated and measured S-parameters of the SPR.

scattering parameters. The Q-points, which were obtained after the calibration process using a matched load and an open load (from the HP 8503B kit), are used to evaluate the SPR performance. **Figs. 9(a–f)** show a comparison between the measured and simulated magnitude and phase of the Q points. The simulation estimated that the Q-point magnitudes vary between 0.5 and 3 across the frequency range of interest. The measurement confirmed this estimation, except for Q3 in the frequency range from 6.5 to 7 GHz, where the magnitude of Q3 exceeds 3. This is attributed to many factors, such as calibration errors in the VNA and fabrication tolerances in the SPR circuit. These factors result in an unexpected change in the measured coupling and isolation corresponding to port 3 within the same range of frequencies, as can be seen in **Figs. 8(c-h)**, respectively. Better results can be achieved by improving the fabrication and calibration processes. **Figs. 9(d–f)** show that the measured phases are inconsistent with the simulated ones in the frequency range from 1 to 5 GHz. This is attributed to the fabrication tolerance that causes slight shifts in the locations of ports 1 to

4. However, this difference does not affect the accuracy of the reflection coefficient estimation because the phase differences among the three Q-points for the simulation and the measurement are comparable at any given frequency.

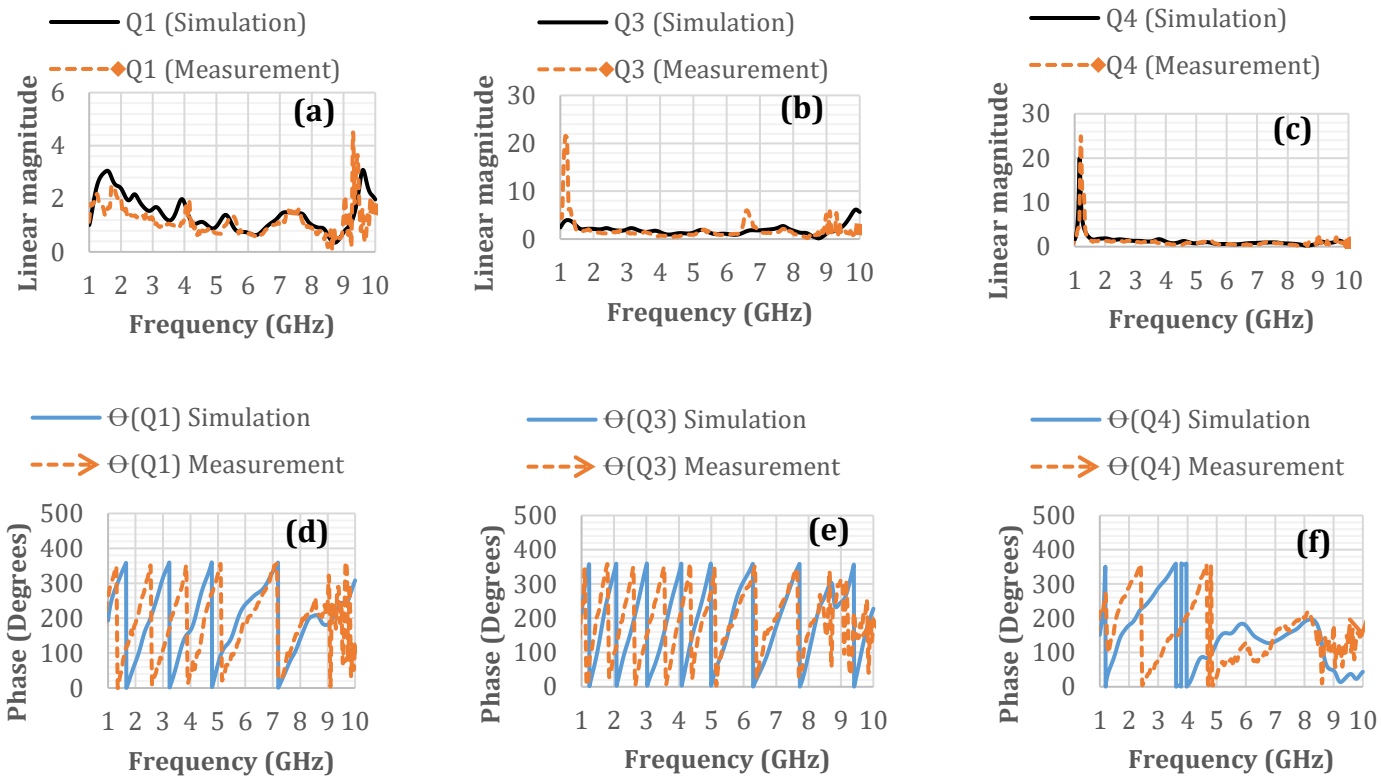

Figure 9. The simulation and measurement results of the SPR Q-point magnitudes and phases: a) |Q1|, b) |Q3|, c) |Q4|, d) Θ(Q1), e) Θ(Q3), and f) Θ(Q4).

To test the proposed SPR, it is required to choose a load that features a reflection coefficient that changes in magnitude and phase at different frequency points within the frequency range of interest. Therefore, a multiband microstrip monopole patch antenna that resonates at 3.5 GHz, 6 GHz, and 7.4 GHz was connected to port 5, and the complex reflection coefficient Γ was estimated using the proposed SPR. By setting the input power connected to port 6 to -5 dBm, the SPR output power at ports (1, 2, 3, and 4) can be measured. The complex reflection coefficient Γ of the antenna was also measured separately using the VNA. The fabricated SPR results demonstrated good agreement with the VNA measurements, as shown in **Figs. 10(a - b)**, except for a minor discrepancy in the frequency range between 6.5 and 7 GHz due to the overshooting of Q3 magnitude. In this range, the phases deviated from the expected values due to the high magnitude of Q3. However, this did not compromise the overall performance of the SPR,

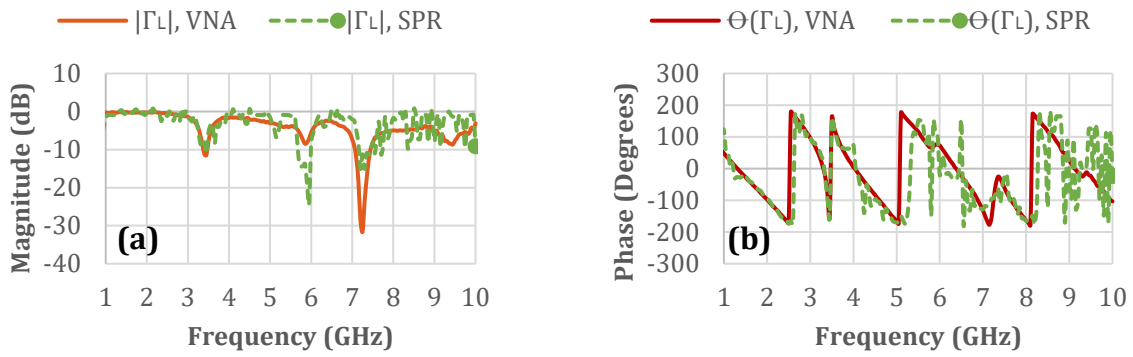

Figure 10. A comparison of the Γʟ measurements between the proposed SPR and the VNA device: (a) |Γʟ|, dB and (b) Θ(Γʟ), degrees.

which was satisfactory up to 8 GHz. **Fig. 11(a)** shows the SPR calibration process performed with the standard open load, and **Fig. 11(b)** depicts the monopole patch antenna connected to the SPR.

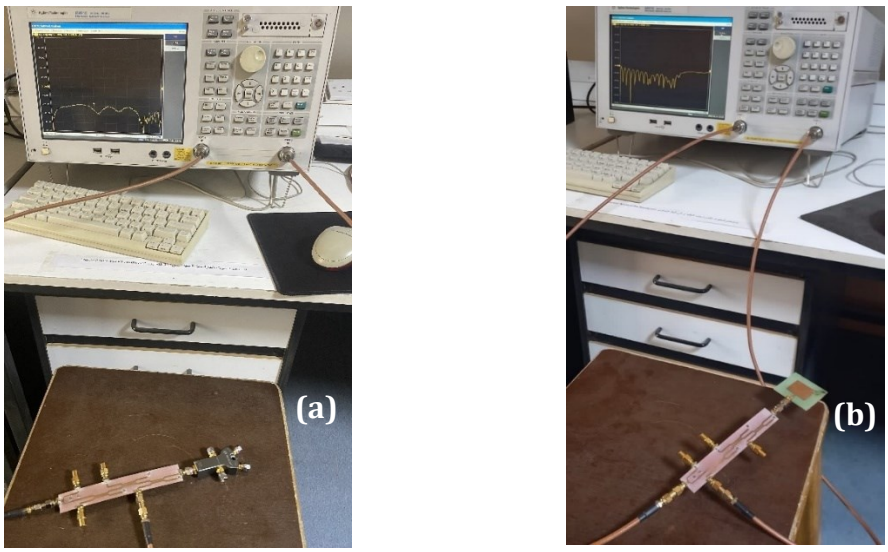

Figure 11. Photograph of the SPR connected to (a) the matched load, and (b) the monopole when measuring the relative power received at one of the ports when the VNA's input signal is applied to the SPR's input.

One of the observations from the experimental results is that the input power level to the DUT beyond 6 GHz (caused by the limited bandwidth of the power divider) has a minimum impact on the calculation of Γ. This implies that the power dissipation in the device does not significantly alter the reflection coefficient estimation at higher frequencies. Therefore, low power can be used for measuring Γ at high frequencies without compromising the accuracy of the measurement. The results have also shown that the algorithm used in the SPR could successfully measure the complex reflection coefficient Γ with high precision and reliability over a wide frequency range, with a compact circuit size and a minimum number of standards. In addition, the proposed SPR showed more accurate results in the presence of high Γ, making it an appropriate choice for many microwave broadband applications. **Table 2** illustrates a comparison between the proposed SPR's performance and those related to similar six-port reflectometers.

Table 2. Performance comparison among previously-reported six-port reflectometers

Reference	Bandwidth (in GHz)	Technology (microstrip, waveguide, multilayer)	No. of calibration standards	Size (in mm)	Measurement range (dB)	Vias	Application
(Staszek et al., 2013)	2 – 3.5	stripline	Four	_	-20~0	No	General purpose
(Staszek et al., 2016)	2.5 – 3.5	stripline	Four	56 x 49	-2~-40	No	General purpose
(Staszek et al., 2017b)	2.2 – 2.6	microstrip	Four	_	-2~-20	No	General purpose
(Ghosh and Kumar, 2017)	1.6 – 2.2	microstrip	Two	126.8 x 19.3	21~39	No	General purpose
(Lin et al., 2017)	2 – 20	multilayer	Three	_	_	Yes	General purpose
(Hassan and Abbas, 2018)	1.75 – 3.25	multilayer	_	_	_	Yes	General purpose
(Odrobina et al., 2018)	1.25 – 4.75	stripline	_	112.5 x 80.4	_	Yes	General purpose
(Staszek, 2022)	5.7 – 5.9	microstrip	several calibration standards	_	-2~-20	No	General purpose
(Peng et al., 2023)	2 – 3	stripline	set of calibration standards	78.9 x 53.6	-2~-20	Yes	General purpose
This work	1 – 8	microstrip	Two	126.8 x 19.3	-15~0	No	microwave broadband applications

5. CONCLUSIONS

In this paper, a six-port reflectometer that features broadband capabilities is presented. The design is based on the use of microstrip multi-section components and a modified design approach to obtain many improvements in terms of size, number of components, and cost. To estimate the complex reflection coefficient (Γ) of an unknown load, a novel algorithm is introduced to improve the estimation accuracy of the proposed design within an extended frequency range. Estimiation of reflection coefficient using the proposed reflectometer shows a good agreement with vector network analyzer (VNA) measurements up to 8 GHz. The proposed design and algorithm can be an important asset in many microwave applications that require broadband complex reflection coefficient measurement.

NOMENCLATURE

Symbol	Description	Symbol	Description
a	The reflected wave from the DUT.	Q_{i}	Complex constant at each port.
A_{i}	Complex calibration constant at ports (1, 2, 3, and 4).	r_{i}	Radius of the three circles (1,3, and 4).
b	The incident wave to the DUT.	S_{56}	The scattering parameter from port 6 to port 5.
b_{i}	Reflected wave at each port, decibels (db).	S_{i5}	The scattering parameter related to the isolation from port 5 to each port.
b_O	The incident wave to the DUT in case of open load is connected.	S_{i6}^{O}	The scattering parameter related to the coupling from port 6 to each port in case of open load is connected to DUT.
B_{i}	Complex calibration constant at ports (1, 2, 3, and 4).	S_{i6}	The scattering parameter related to the coupling from port 6 to each port.
C_{i}	Real constants.	Γ	Complex reflection coefficient, db.
Centroid	The centroid of triangle.	Γ_O	Complex reflection coefficient of the open load, db.
d	The Euclidean distance between any two intersections.	Γ_L	Complex reflection coefficient of the load, db.
P_{i}	Power detected at each port, milliwatt (mw).	ε_r	Dielectric constant, unitless.

Acknowledgements

The authors would like to thank Dr. Lubab Ali Salman from Al Nahrain University for his help and support in performing the measurements for the fabricated circuit.

Credit Authorship Contribution Statement

Nadine Adnan: Writing, design and modelling methodology, editing.
Ghassan Nihad Jawad: Reviewing and proofreading.

Declaration of Competing Interest

The authors declare that they have no known competing financial interests or personal relationships that could have appeared to influence the work reported in this paper.

REFERENCES

Abbass, S.J. and Abdulateef, E.F.M.R., 2012. Finite element analysis of human and artificial articular cartilage. *Journal of Engineering*, 18(4), pp. 443-458. Doi:10.31026/j.eng.2012.04.06.

Aishah, S., Fareq, M., Cheng, E., Lee, K., Tan, W., Afendi, M., Shahriman, A., Nasir, N. M., Tan, W. and Syahirah, K., 2015. Study on moisture content in animal fats using Six-Port Reflectometer (SPR). *2015 2nd International Conference on Biomedical Engineering (ICoBE)*. IEEE, pp. 1-5. Doi:10.1109/ICoBE.2015.7235920.

Al-Jumaily, A. and Al-Ammri, A. S., 2009. Analysis of wave propagation in detection of aorta dieses using lumps analysis. *Al-Khwarizmi Engineering Journal*, 5(3), pp. 16-22. https://alkej.uobaghdad.edu.iq/index.php/alkej/article/view/566.

Ali, H. O. and Al-Hindawi, A. M., 2021. A Ultra-broadband Thin metamaterial absorber for Ku and K bands applications. *Journal of Engineering*, 27(5), pp. 1-16. Doi:10.31026/j.eng.2021.05.01.

Bialkowski, M. E., Abbosh, A. M. and Seman, N., 2007. Compact microwave six-port vector voltmeters for ultra-wideband applications. *IEEE Transactions on Microwave Theory and Techniques*, 55(10), pp. 2216-2223. Doi:10.1109/TMTT.2007.906539.

Bilik, V., 2002. Six-port measurement technique: Principles, impact, applications. *Invited paper at the International Conference Radioelektronika*. https://www.yumpu.com/en/document/view/5389511/six-port-measurement-technique-s-team-lab.

Brunetti, L., 1990. Geometrical estimator use in six-port reflectometer study. *Conference on Precision Electromagnetic Measurements*. IEEE, pp. 402-403. Doi:10.1109/CPEM.1990.110079.

Brunetti, L., Fornero, C. and Rietto, G., 1989. Six-port reflectometer: influence of Q-points position in Gamma-plane on sidearm power detector error propagation. *IEEE Transactions on Instrumentation and Measurement*, 38(2), pp. 484-487. Doi:10.1109/19.192332.

Dietrich, F., Wei, M.-D. and Negra, R., 2018. Low-Cost, Wideband multiport reflectometer in single-layer structure for accurate high VSWR measurement. *2018 91st ARFTG Microwave Measurement Conference (ARFTG)*. IEEE, pp. 1-4. Doi:10.1109/ARFTG.2018.8423819.

Engen, G. F., 1977a. An improved circuit for implementing the six-port technique of microwave measurements. *IEEE Transactions on microwave theory and techniques*, 25(12), pp. 1080-1083. Doi:10.1109/TMTT.1977.1129278.

Engen, G. F., 1977b. The six-port reflectometer: An alternative network analyzer. *IEEE Transactions on microwave theory and techniques*, 25(12), pp. 1075-1080. Doi:10.1109/TMTT.1977.1129277.

Engen, G. F., 1992. *Microwave circuit theory and foundations of microwave metrology*, IET. https://books.google.iq/books/about/Microwave_Circuit_Theory_and_Foundations.html?id=-SL-oDSRQ7cC&redir_esc=y.

Ghannouchi, F. M. and Mohammadi, A., 2009. *The six-port technique with microwave and wireless applications*, Artech House. https://books.google.iq/books?id=-t0fu4zpMh0C&printsec=copyright&redir_esc=y#v=onepage&q&f=false.

Ghosh, D. and Kumar, G., 2017. Six-port reflectometer using edge-coupled microstrip couplers. *IEEE Microwave and Wireless Components Letters*, 27(3), pp. 245-247. Doi:10.1109/LMWC.2017.2661708.

Haddadi, K., Loyez, C., Clavier, L., Pomorski, D. and Lallemand, S., 2018. Six-port reflectometer in WR15 metallic waveguide for free-space sensing applications. *2018 IEEE Topical Conference on Wireless Sensors and Sensor Networks (WiSNet)*. IEEE, pp. 80-83. Doi:10.1109/WISNET.2018.8311570.

Haddadi, K., Wang, M., Glay, D. and Lasri, T., 2008. Ultra wide-band four-port reflectometer using only two quadratic detectors. *2008 IEEE MTT-S International Microwave Symposium Digest*. IEEE, pp. 379-382. Doi:10.1109/MWSYM.2008.4633182.

Hassan, A. and Abbas, O., 2018. Design of a wide band six port reflectometer using broadside coupled lines. *Microwave and Optical Technology Letters*, 60(9), pp. 2101-2103. Doi:10.1002/mop.31310.

Hathal, M. S., Salih, S. S. and Hasan, A. H., 2021. Ultra-wideband featuring enhanced delay and sum algorithm and oriented for detecting early stage breast cancer. *Progress In Electromagnetics Research M*, 100, pp. 141-150. Doi:10.2528/PIERM20012804.

Issa, R. S., Almamori, A. and Al Hamdani, H., 2022. Broadband reflectarray design for wireless applications. *2022 International Conference on Electrical, Computer and Energy Technologies (ICECET)*. IEEE, pp. 1-4. Doi:10.1109/ICECET55527.2022.9872838.

Jawad, G. N. and Akbar, M. F., 2021. IFFT-based microwave non-destructive testing for delamination detection and thickness estimation. *IEEE Access*, 9, pp. 98561-98572. Doi:10.1109/ACCESS.2021.3095105.

Lin, T., Gu, S. and Lasri, T., 2017. 2-20 GHz non-uniform coupler for six-port reflectometer. *2017 IEEE Topical Conference on Wireless Sensors and Sensor Networks (WiSNet)*. IEEE, pp. 15-18. Doi:10.1109/WISNET.2017.7929775.

Mishra, B., Rahman, A., Shaw, S., Mohd, M., Mondal, S. and Sarkar, P., 2014. Design of an ultra-wideband Wilkinson power divider. *2014 First International Conference on Automation, Control, Energy and Systems (ACES)*. IEEE, pp. 1-4. Doi:10.1109/ACES.2014.6807987.

Mohammed, B. S., Ahmed, E. S. and Sateaa, S. D., 2014. The mutual Interaction effects between Array Antenna Parameters and Receiving Signals Bandwidth. *Al-Khwarizmi Engineering Journal*, 10(1), pp. 83-91. https://alkej.uobaghdad.edu.iq/index.php/alkej/article/view/193.

Odrobina, S., Staszek, K., Wincza, K. and Gruszczynski, S., 2017. Measurement uncertainty analysis and design of a broadband four-port reflectometer. *IET Microwaves, Antennas & Propagation*, 11(15), pp. 2162-2167. Doi:10.1049/iet-map.2017.0435.

Odrobina, S., Staszek, K., Wincza, K. and Gruszczynski, S., 2018. Wideband six-port reflectometer. *2018 14th International Conference on Advanced Trends in Radioelecrtronics, Telecommunications and Computer Engineering (TCSET)*. IEEE, pp. 597-601. Doi:10.1109/TCSET.2018.8336273.

Peng, S., Li, Z., Jing, R., Zhu, H. and Hong, T., 2023. Quasi-optimal and optimal six-port reflectometers using coupled-line directional couplers. *IEEE Transactions on Instrumentation and Measurement*. Doi:10.1109/TIM.2023.3317382.

Pozar, D. M., 2012. Microwave engineering. *Fourth Editions, University of Massachusetts at Amherst, John Wiley & Sons, Inc*, pp. 26-30. https://www.wiley.com/en-us/Microwave+Engineering%2C+4th+Edition-p-9780470631553.

Seman, N., Bialkowski, M. E. and Khor, W. C., 2008. Fully integrated UWB microwave reflectometer in multi-layer microstrip-slot technology. *2008 Asia-Pacific Microwave Conference*. IEEE, pp. 1-4. Doi:10.1109/APMC.2008.4957894.

Shrifan, N. H., Jawad, G. N., Isa, N. A. M. and Akbar, M. F., 2020. Microwave nondestructive testing for defect detection in composites based on K-means clustering algorithm. *IEEE Access*, 9, pp. 4820-4828. Doi:10.1109/ACCESS.2020.3048147.

Staszek, K., 2022. Six-Port reflectometer insensitive to power detectors' impedance mismatch. *IEEE Access*, 10, pp. 89072-89082. Doi:10.1109/ACCESS.2022.3201126.

Staszek, K., Gruszczynski, S. and Wincza, K., 2013. Design and accuracy analysis of a broadband six-port reflectometer utilizing coupled-line directional couplers. *Microwave and Optical Technology Letters*, 55(7), pp. 1485-1490. http://dx.doi.org/10.1002/mop.27630.

Staszek, K., Gruszczynski, S. and Wincza, K., 2016. Six-port reflectometer providing enhanced power distribution. *IEEE Transactions on Microwave Theory and Techniques*, 64(3), pp. 939-951. Doi:10.1109/TMTT.2016.2518681.

Staszek, K., Gruszczynski, S. and Wincza, K., 2017a. Ultra-wideband dual-line multiprobe reflectometer. *IEEE Transactions on Microwave Theory and Techniques*, 65(4), pp. 1324-1333. Doi:10.1109/TMTT.2016.2638422.

Staszek, K., Sorocki, J., Wincza, K. and Gruszczyński, S., 2017b. Six-port reflectometer with tunable parameters ensuring measurement accuracy enhancement. *2017 IEEE Topical Conference on Wireless Sensors and Sensor Networks (WiSNet)*. IEEE, pp. 26-29. Doi:10.1109/WISNET.2017.7878747.

Steer, M., 2019. *Microwave and RF design*, NC State University. https://uncpress.org/book/9781469656885/fundamentals-of-microwave-and-rf-design/.

Yeo, S. and Lee, K., 1990. Improvements in design of six-port reflectometer comprising symmetrical five-port waveguide junction and directional coupler. *IEEE transactions on instrumentation and measurement*, 39(1), pp. 184-188. Doi:10.1109/19.50441.

Zoughi, R., 2000. *Microwave non-destructive testing and evaluation principles*, Springer Science & Business Media. https://link.springer.com/book/10.1007/978-94-015-1303-6.